# Correlation of Peak Dynamic and Static Coulomb Failure Stress with Seismicity Rate Change after the Mw7.2 El Mayor-Cucapah Earthquake

Kyle B. Withers and Kim B. Olsen

February 29, 2012

Department of Geological Sciences, San Diego State University, San Diego, CA 92182-1020

## Summary of Major Research Findings

We have investigated the relation between the April 4 Mw7.2 El Mayor-Cucapah earthquake and seismicity rate changes in southern California and northern Baja California in the months following the mainshock. Specifically, we use a dynamic rupture model with observational constraints for the event simulated in the SCEC 3D CVM4.0 (Roten and Olsen, 2009) to calculate the changes in the resulting static (dCFS) and dynamic Coulomb failure stress, parametrized by its largest positive amplitude (peak dCFS(t)). We employ a modified cross correlation between the seismicity rate change (for both undeclustered and declustered catalogs) and both dCFS and peak dCFS(t) in time and space (as used by Kilb et. al, 2002). We find that the correlation parameter is greater for peak dCFS(t) compared to dCFS and highest for periods after the mainshock of longer than 1 week for dCFS, and a maximum at 1 month for peak dCFS(t). We perform this analysis using both CVM-4 and CVM-H, investigating, in particular, which model better describes the increased seismicity NW of the rupture. The stress changes are rotated onto the focal mechanism of the June 15, 2010 Mw5.7 aftershock as well as onto optimum oriented planes (King, 1994). For regionally rotated stresses we find that while the dCFS values are very similar for the two CVMs, the corresponding peak dCFS(t) values are noticeably different. In particular, CVM-H generates a lobe of (directivity-induced) large peak dCFS(t) between the Elsinore and San Jacinto Faults toward the Los Angeles basin not present in the results from CVM-4. However, both CVMs produce similar peak dCFS(t) lobes near San Diego. Finally, we searched for threshold levels of dCFS and peak dCFS(t) that may be required to trigger earthquakes/aftershocks of different magnitude that might provide clues to earthquake prediction; we found a possible peak dCFS(t) threshold value of 0.7 bars for aftershocks (>4000) in regions of positive static stress.

## Introduction

We have investigated the relation between the April 4 Mw7.2 El Mayor- Cucapah earthquake and seismicity rate changes in southern California and northern Baja California in the months following the mainshock. Specifically, we use a dynamic rupture model with observational constraints for the event simulated in the SCEC 3D CVM4.0 (Roten and Olsen, 2009) to calculate the changes in the resulting static (dCFS) and dynamic Coulomb failure stress, dCFS(t), parametrized by its largest positive amplitude (peak dCFS(t)). We employ a modified cross correlation between the seismicity rate change (for both undeclustered and declustered catalog) and both dCFS and peak dCFS(t) in time and space (as used by Kilb et. al, 2002). We perform this analysis using both CVM-4 and CVM-H v6.2, investigating, in particular, which model better describes the increased seismicity NW of the rupture. The stress changes are rotated onto the focal mechanism of the June 15, 2010 Mw5.7 aftershock as well as onto optimum oriented planes (King, 1994). Finally, we searched for threshold levels of static or dynamic stress changes that may be required to trigger earthquakes/aftershocks of different magnitude that might provide clues to earthquake prediction.

## Static Versus Dynamic Coulomb Failure Stress

Coulomb failure stress can be used as a criterion to show conditions under which failure will occur in rocks. Coulomb failure stress is defined as: $\sigma_f = \tau_\beta + \mu(\sigma_\beta + p)$ , where $\tau_\beta$ is the shear stress on the failure plane, $\sigma_\beta$ is the normal stress, $p$ is the pore fluid pressure and $\mu$ is the coefficient of friction. Static Coulomb stress changes are defined as permanent and depend on the final fault offset. Alternately, dynamic Coulomb failure stresses are dependent on the rupture process and vary over time (Figure 1) (Kilb et al., 2002). In this study we use $\mu = 0.4$; while largely unconstrained, the static and dynamic stress changes are only slightly sensitive to $\mu$ values between 0.2 and 0.6 (see Doser et al., 2009).

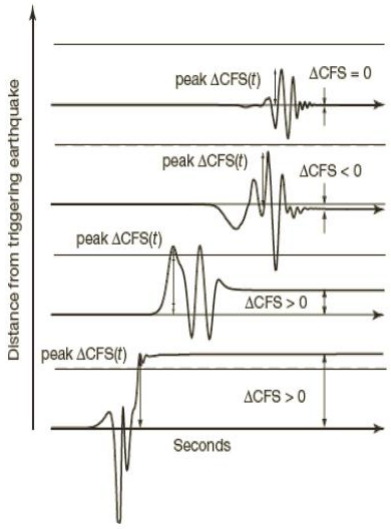


Figure 1. The progression of the complete Coulomb stress change, ΔCFS(t), over time and distance. The double arrows show the peak ΔCFS(t), or dynamic stress values, and the static Δ CFS, which can be positive or negative. [From Kilb et al., 2000]

## Rupture Model

We used a dynamic rupture model constrained by fault geometry, rake, hypocenter location and reported surface displacement (using Roten and Olsen (2010)). Dynamic rupture was simulated assuming depth-dependent normal stress (Dalguer and Mai, 2008) and emulated velocity strengthening near the free surface using the SGSN FD method on a planar vertical fault. Our rupture model features surface

slip of up to 2.0 m NW of the hypocenter, with buried slip under the Colorado River Delta SE of the hypocenter.

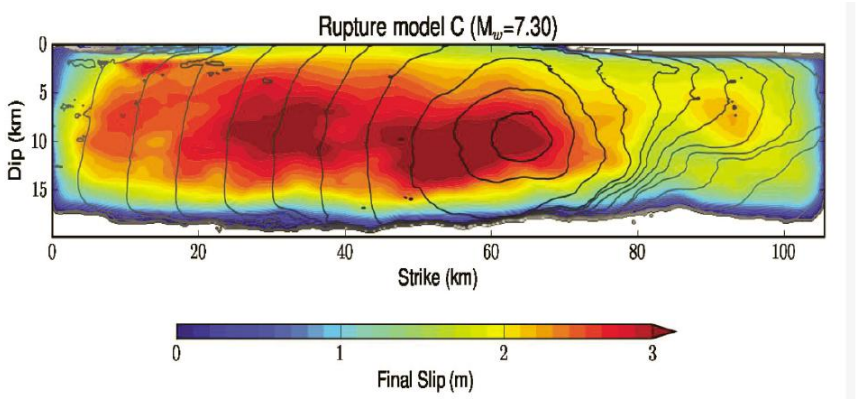


Figure 2. Final slip on the fault obtained in the rupture model used.

## Static and Peak Dynamic Stresses for El-Mayor Cucupah Earthquake

Static CFS and peak dCFS are modeled using a fourth-order staggered-grid finite difference method (AWP-ODC), which incorporates anelastic attenuation, a 3-D velocity model (both CVM-4 and CVM-H), and a heterogeneous slip distributions derived from dynamic rupture modeling, producing 0-1.5 Hz ground motions in general agreement with recorded strong motion data. The model grid is 280 by 280 km with a grid spacing of 100 m. The stresses were calculated at a depth of 5 km, which correspond to the depth level containing most of the aftershock seismicity. The 0-1.5 Hz stress changes were calculated on the Kraken Supercomputer at NICS using 3920 processors requiring about 8 wall-clock hours. In Figure 3, shown below, static and peak dynamic stress changes calcualted from CVM-4 are rotated onto a strike of 310 degrees, corresponding to the rupture of the Mw 5.72 June 15, 2010 event. It is evident that there is strong directivity of the peak dynamic stress changes toward NW, absent in the static stress changes.

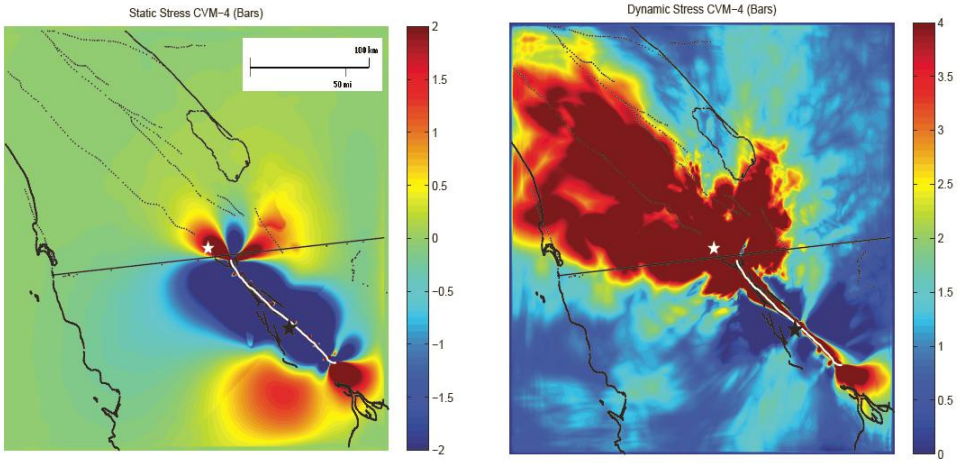


Figure 3. (left) Static and (right) peak dynamic stress changes (in bars) calculated from CVM-4, rotated onto a strike of 310 degrees, corresponding to the rupture of the Mw 5.72 June 15, 2010 event (epicenter depicted by the white star, mainshock by black star).

### Coulomb Stress changes Calculated from CVM-4 and CVM-H

Both sCFS and peak dCFS were resolved on optimally oriented failure planes by adding a 10 bar regional compressive stress, oriented N7E, to the earthquake induced stresses (King 1994) for CVM-4 and CVM-H (shown in Figure 4). While the static stress changes are very similar for the two CVM's, the corresponding peak dynamic stress changes are noticeably different. In particular, CVM-H generates a lobe of (directivity-induced) large peak dynamic stress changes between the Elsinore and San Jacinto Faults toward the Los Angeles basin, not present in the results from CVM-4.

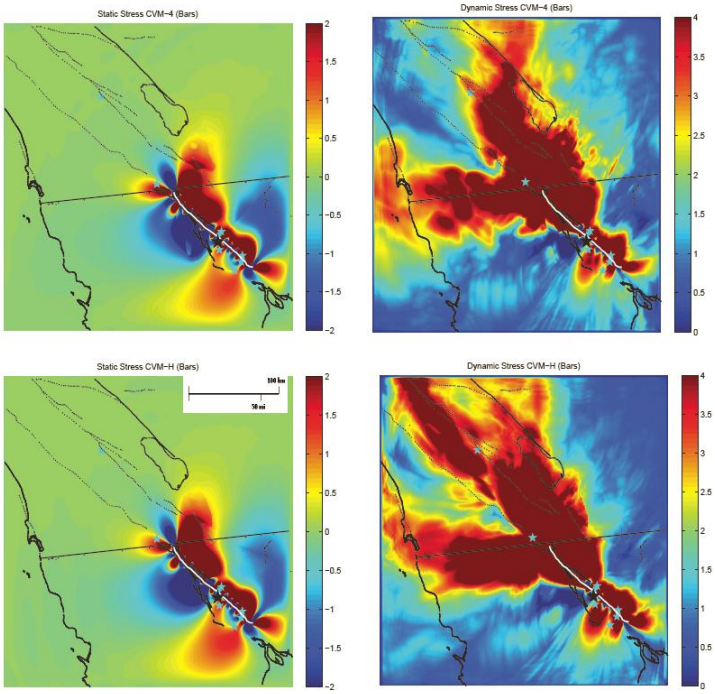


Figure 4. Static and dynamic stresses calculated from (left) CVM-4 and (right) CVM-H, regionally rotated, with Mw>5 aftershocks superimposed, along with major faults, coastline, and bodies of water.

## Seismicity Rate Change

Seismicity rate change was calculated as the ratio of events in a period after the mainshock to a background period prior to the mainshock using a log-scale. This scale is transformed so that a positive ratio indicates an increase in seismicity rate change (SRC) while a negative ratio indicates a decrease in SRC.

We constructed SRC maps calculated for 1 day, 1 week, 1 month, 3 months and 1 year after the mainshock (for both declustered and undeclustered catalogs) using a background period prior to the mainshock event from Jan 1 2008 to Mar 15 2010. This background period was selected since it included no foreshocks or changes in aftershock reporting or recording and appeared to best represent the seismicity rate prior to the mainshock. Since the highest magnitude of completeness (Mc) calculated for all the aftershock and background periods was 1.5, both background and aftershock seismicity rate change only included events for which Mw >1.5. This Mc was applied to help remove background seismicity and to minimize the effects of any secondary aftershocks (earthquakes triggered by other neighboring aftershocks).

The study area was divided into a grid with a spacing of 0.05 latitude and longitude. A circular area with radius of 5 km was used around each grid point in order to include a reasonable number of earthquakes with magnitude larger than Mc. This radius was chosen because it provided the most reliable and accurate spatial coverage out of all the radii experimented.

The SRC maps were overlain on the stress maps to calculate the correlation coefficient. A cross-

correlation measure was chosen because it takes into account the gradients of the stress and seismicity rate changes. All SCFS models provided negative correlation with seismicity rate change for all time periods because of the anti-correlation with the stress shadow or area of negative sCFS. This anti-correlation was due to the absence of seismicity rate decreases, which made it difficult to provide a fair comparison between sCFS to peak dCFS using triggering seismicity rate change. Thus, only positive sCFS values were correlated with SRC.

## Correlation of Seismicity Rate Change with Stresses

We used a modified cross correlation technique to calculate the correlation between seismicity range change and stress values (as performed in Kilb, et. al. 2002). For different periods of interest, ranging from 1 day to 1 year after the mainshock, we looped through threshold values of stress (i.e. setting the stress equal to the threshold value if it lies above it) and extracted the highest correlation coefficient (R) for all threshold values and the associated significance, defined by: $t = R * \sqrt{\frac{n-2}{1-R^2}}$. The significance critical value for degrees of freedom (df) = 120 (the number of points in the correlation) is 1.658 for the 95% confidence level using a one-tailed test. The null hypothesis can be rejected if the significance value is above this. The results for periods using CVM-4 undeclustered are shown in Table 1, below. This table shows that high correlation coefficients (R > 0.40) with seismicity rate change a month after the mainshocks, with decreasing correlation for shorter time periods. We find that the correlation parameter is greater for peak dCFS(t) compared to dCFS and highest for periods after the mainshock of longer than 1 week for dCFS, and a maximum at 1 month for peak dCFS(t).

| | 1 Day | | 1 Week | | 1 Month | | 3 Month | | 1 Year | |
|---|---|---|---|---|---|---|---|---|---|---|
| | Static | Dynamic | Static | Dynamic | Static | Dynamic | Static | Dynamic | Static | Dynamic |
| R | 0.016 | 0.082 | 0.123 | 0.190 | 0.141 | 0.223 | 0.164 | 0.252 | 0.181 | 0.190 |
| Threshold Value (bars) | 0.699 | 7.131 | 0.209 | 11.582 | 0.323 | 12.985 | 0.648 | 12.984 | 0.092 | 16.081 |
| R Value at Threshold | 0.179 | 0.165 | 0.226 | 0.238 | 0.391 | 0.337 | 0.458 | 0.486 | 0.462 | 0.468 |
| Signicance | 1.634 | 1.507 | 2.285 | 2.414 | 4.437 | 3.669 | 5.349 | 5.773 | 8.340 | 8.479 |

Table 1. Correlation results between seismicity rate change and both sCFS and dCFS for various time periods after the mainshocks for undeclustered CVM-4. R is the correlation coefficient without using a threshold value.

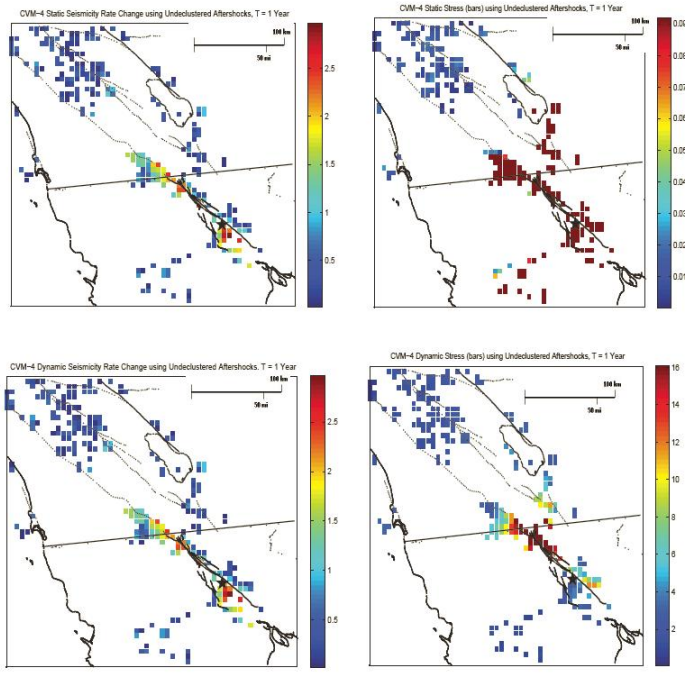


Figure 5. Seismicity (left) rate- and (right) stress changes for static (top) and dynamic (bottom) at the estimated stress change threshold value for CVM-4 providing the best correlation (see Table 1) for a period after the mainshock of 1 month.

## Dynamic Threshold Triggering of Aftershocks

Figure 6, below, plots magnitude versus depth for dynamic and static stress changes. This figure indicates a potential threshold level (0.7 bars) of dCFS required to trigger earthquakes/aftershocks of different magnitude that might help to define earthquake locations in the future. The selected aftershocks plotted in Figure 4 are limited to locations up to a month after the mainshock, where the regional rotated static stress is positive for CVM-4. A threshold value was not seen in locations where static stress was negative, nor the aftershock locations where static stress was positive.

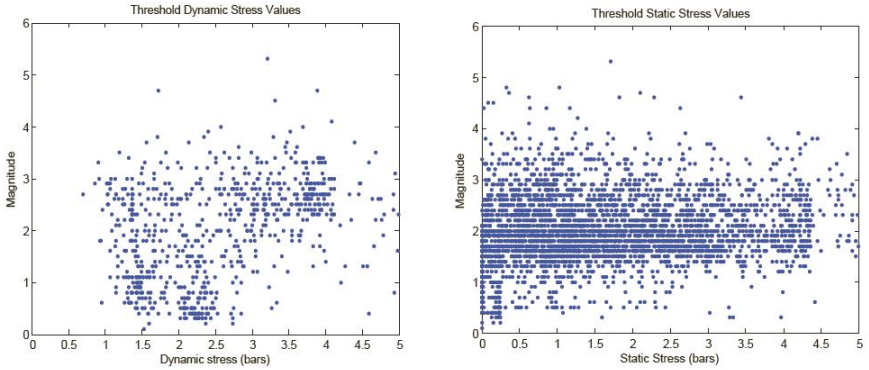


Figure 6. Magnitude versus depth (left) for dynamic and (right) static stress changes at the locations of aftershocks ($>$ 4000) up to 1 month after the mainshock, suggesting the presence of a dynamic threshold value of 0.7 bars.

## Conclusions

We have modeled static CFS and peak dCFS for the Mw7.2 El Mayor-Cucapah Earthquake using a fourth-order staggered-grid finite difference method (AWP-ODC). Our results show that the undeclustered catalog of aftershocks of the El Mayor-Cucapah earthquake provides significantly better correlation with seismicity rate change than the declustered catalog for almost all time periods for both CVM-4 and CVM-H. For regionally rotated stresses we find that while the dCFS values are very similar for the two CVMs, the corresponding peak dCFS(t) values are noticeably different. In particular, CVM-H generates a lobe of (directivity-induced) large peak dCFS(t) between the Elsinore and San Jacinto Faults toward the Los Angeles basin, which is not present in the results from CVM-4. However, both CVMs produce similar peak dCFS(t) lobes near San Diego.

Both sCFS and peak dCFS provide high correlation coefficients (R $>$ 0.40) with seismicity rate change a month after the mainshocks, with decreasing correlation for shorter time periods using the undeclustered catalog. We find that the correlation parameter is greater for peak dCFS(t) compared to dCFS and highest for periods after the mainshock of longer than 1 week for dCFS, and a maximum at 1 month for peak dCFS(t). CVM-H is seen to have a higher correlation (on average) than CVM-4 at periods of 1 month or less for both undeclustered and declustered catalogs.

We recommend that both sCFS and peak dCFS should be incorporated in studies of stress transfer and earthquake triggering, as they both appear to affect aftershock seismicity in a complementary way and show varying goodness of fit values with different time periods after the mainshock (ranging from a day to 1 year). We find that increases in static stress changes closer to the fault can explain nearby aftershocks, while the triggering of those farther away are more likely attributed to dynamic stress changes, where static stress change is nearly zero. We have found a possible peak dCFS(t) threshold value of 0.7 bars for aftershocks ($>$4000) in regions of positive static stress required to trigger earthquakes/aftershocks of different magnitude that might help to define earthquake locations in the future.

# References


Árnadóttir, Th., S. Jónsson, R. Pedersen, and G.B. Gudmundsson (2003). Coulomb stress changes in the South Iceland Seismic Zone due to two large earthquakes in June 2000, AGU-EUG-EGS Joint assembly,Abstract G12-1TU4O-002, Nice, April 6-11, France.

Chouliaras, G., Stavrakakis, G.N. (2001). Current seismic quiescence in Greece: implications for seismic hazard. J. Seismol. 5, 595–608.

Dalguer, L.A. and Mai, M. (2008). Implications of Style-of-Faulting and Loading Characteristics on the Dynamic Rupture Process, AGU Fall Meeting Abstracts, 1798.

Doser, D.I., K.B. Olsen, F.F. Pollitz, R.S. Stein, and S. Toda (2009). The 1911 M~6.6 Calaveras earthquake: Source parameters and the role of static, viscoelastic and dynamic Coulomb stress changes imparted by the 1906 San Francisco earthquake, Bull. Seis. Soc. Am. 99, 1746-1759.

Du, W., L. R. Sykes, B. E. Shaw, and C. H. Scholz (2003). Triggered a seismic fault slip from nearby earthquakes, static or dynamic effect?, J. Jiffies. Res., 108, 2131, do:10.1029/2002JB002008.

Freed A.M. (2005). Earthquake triggering by static, dynamic, and postseismic stress transfer Annu. Rev. Earth Planet. Sci., 33, p.335-367.

Habermann, R.E. (1983). Teleseismic detection in the Aleutian Island arc, J. Geophys. Res., 88, 5056-5064.

Kilb, D. (2002). A strong correlation between induced peak dynamic Coulomb stress change from the 1992 M7.3 Landers, California, earthquake and the hypocenter of the 1999 M7.1 Hector Mine, California, earthquake, J. Geophys. Res., 107, doi:10.1029/2001JB000678.

Kilb, D., J. Gomberg, and P. Bodin (2000). Triggering of earthquake aftershocks by dynamic stresses, Nature, 408, 570-574.

Kilb, D., J. Gomberg, and P. Bodin (2002). Aftershock triggering by complete Coulomb stress changes, J. Geophys. Res., 107, 2001JB000202.

King G. C. P., R. S. Stein, and J. Lin (1994). Static stress changes and the triggering of earthquakes, Bull. Seismol. Soc. Am., 84, 935-953.

Roten, D. and Olsen, K.B. (2010). Simulation of Ground Motion in the Imperial Valley Area During the Mw 7.2 El Mayor-Cucapah Earthquake. Proceedings of the Annual SCEC meeting, Palm Springs, September 2010, 1-069, p. 169.

Stein, R. S., G. C. P. King, and J. Lin (1992). Change in failure stress on the southern San Andreas fault system caused by the 1992 Magnitude=7.4 Landers earthquake, Science, 258, 1328-1332.

Toda, S. and Stein, R.S. (2002). Response of the San Andreas Fault to the 1983 Coalinga-Nuñez Earthquakes: An Application of Interaction-based Probabilities for Parkfield, J. Geophys. Res. 107, 10.1029/2001JB000172.

Wiemer, S. and F.R. Zuniga (1994). ZMAP-a software package to analyze seismicity. EOS, Transactions, Fall Meeting, AGU, 75, 456.

**Publications Supported by SCEC3 funds (not just this award):**


Cui, Y., K.B. Olsen, T. H. Jordan, K. Lee, J. Zhou, P. Small, D. Roten, G. Ely, D.K. Panda, A. Chourasia, J. Levesque, S. M. Day, P. Maechling (2010). Scalable earthquake simulation on petascale supercomputers, Gordon Bell Prize finalist, and in Procs. Supercomputing Conference, New Orleans, November 2010

Cruz-Atienza, V.M., and K.B. Olsen, K.B. (2010). Supershear Mach-waves expose the fault breakdown slip, *Tectonophysics* , pp 1-12, doi:10.1016/j.tecto.2010.05.012.

Olsen, K.B., and J.E. Mayhew (2010). Goodness-of-fit Criteria for Broadband Synthetic Seismograms, With Application to the 2008 Mw5.4 Chino Hills, CA, Earthquake, *Seism. Res. Lett.* **81** , 715-723.

Bielak, J., R.W. Graves, K.B. Olsen, R. Taborda, L. Ramirez-Guzman, S.M. Day, G.P. Ely, D. Roten, T.H. Jordan, P.J. Maechling, J. Urbanic, Y. cui, and G. Juve (2010). The ShakeOut earthquake scenario: Verification of three simulation sets, *Geophysical Journal International* **180**, 375-404, doi: 10.1111/j.1365-246X.2009.04417.x.

Mai, P.M., W. Imperatori, and K.B. Olsen (2010). Hybrid broadband ground-motion simulations: combining long-period deterministic synthetics with high-frequency multiple S-to-S back-scattering, *Bull. Seis. Soc. Am.* **100**, 5A, 2124-2142.

Mena, B., P.M. Mai, K.B. Olsen, M.D. Purvance, and J.N. Brune (2010). Hybrid broadband ground motion simulation using scattering Green's functions: application to large magnitude events, *Bull. Seis. Soc. Am.* **100**, 5A, 2143-2162.

Cui, Y., Chourasia, A., Moore, R., Olsen, K., Maechling, P., Jordan, T. (2009). The TeraShake Computational Platform for Large-scale Earthquake Simulations, Advances in Geocomputing, *Lecture Notes in Earth Sciences* **119**, DOI 10.1007/978-3-540-85879-9_7, pp229-278, editor H. Xing, Springer-Verlag Berlin Heidelberg.

Cruz-Atienza, V.M., K.B. Olsen, and L.A. Dalguer (2009). Estimation of the breakdown slip from strong-motion seismograms: insights from numerical experiments *Bull. Seis. Soc. Am.* **9**, 3454-3469, doi:10.1785/0120080330.

Olsen, K.B., and G. Ely (2009). WebSims: A Web-based System for Storage, Visualization, and Dissemination of Earthquake Ground Motion Simulations, *Seismol. Res. Lett.* **80**, 1002-1007, doi:10.1785/gssrl.80.6.1002

Olsen, K. B., S. M. Day, L. Dalguer, J. Mayhew, Y. Cui, J. Zhu, V.M. Cruz-Atienza, D. Roten, P. Maechling, T.H. Jordan, and A. Chourasia (2009). ShakeOut-D: Ground Motion Estimates Using an Ensemble of Large Earthquakes on the Southern San

Andreas Fault With Spontaneous Rupture Propagation, *Geophysical Research Letters* **36** L04303, doi:10.1029/2008GL036832.

Harris, R.A., M. Barall, R. Archuleta, E. Dunham, B. Aagaard, J.P. Ampuero, H., Bhat, V. Cruz-Atienza, L. Dalguer, P. Dawson, S. Day, B. Duan, G. Ely, Y., Kaneko, Y. Kase, N. Lapusta, Y. Liu, S. Ma, D. Oglesby, K. Olsen, A. Pitarka, S. Song, E. Templeton (2008). The SCEC/USGS dynamic earthquake-rupture code verification exercise, *Seism. Res. Lett.* **80**, Vol 1, 119-126, DOI:10.1785/gssrl.80.1.119

Olsen, K.B., W.J. Stephenson, and Andreas Geisselmeyer (2008). 3D Crustal Structure and Long-period Ground Motions From a M9.0 Megathrust Earthquake in the Pacific Northwest Region, *Jour. Seismol.* DOI 10.1007/s10950-007-9082.

Olsen, K.B. and J.N. Brune (2008). Constraints from precariously balanced rocks on preferred rupture directions for large earthquakes on the southern San Andreas Fault, *Jour. Seismol.* DOI 10.1007/s10950-007-9078-7.

Olsen, K.B., S. M. Day, J. B. Minster, Y. Cui, A Chouasia, R. Moore, P. Maechling, T. Jordan (2008), TeraShake2: simulation of Mw7.7 earthquakes on the southern San Andreas fault with spontaneous rupture description, *Bull. Seismol. Soc. Am.* **98**, 1162-1185, doi: 10.1785/0120070148.

Day, S. M., R. W. Graves, J. Bielak, D. Dreger, S. Larsen, K. B. Olsen, A. Pitarka, and L. Ramirez-Guzman (2008). Model for basin effects on long-period response spectra in southern California, *Earthquake Spectra* **24**, 257-277.

A. Chourasia, S. M. Cutchin, K. B. Olsen, B. Minster, S. Day, Y. Cui, P. Maechling, R. Moore, T. Jordan (2007). Visual insights into high-resolution earthquake simulations, IEEE Computer Graphics and Applications (Discovering the Unexpected) vol. 27, no. 5, Sep-Oct issue.

Cui, Y., R. Moore, K., K. Olsen, A. Chourasia, P. Maechling, J.B. Minster, S. Day, Y. Hu, J. Zhu, A. Majundar, and T. Jordan (2007). Enabling very large scale earthquake simulations on parallel machines, Advancing Science and Society through Computation, Lecture Notes in Computer Science series, International Conference on Computational Science, 46-53, Springer.

Olsen, K. B., S. M. Day, J. B. Minster, Y. Cui, A. Chourasia, M. Faerman, R. Moore, P. Maechling, and T. Jordan (2006). Strong shaking in Los Angeles expected from southern San Andreas earthquake, *Geophysical Research Letters*, **33**, L07305, doi:10.1029/2005GL025472.